High-Performance Luminescence Thermometer with Field-Induced Slow Magnetic Relaxation Based on a Heterometallic Cyanido-Bridged 3d−4f Complex

Vassilis Tangoulis,* Vassilis Nastopoulos, Nikos Panagiotou, Anastasios Tasiopoulos, Grigorios Itskos,* Modestos Athanasiou, Eufemio Moreno-Pineda, Wolfgang Wernsdorfer,* Michael Schulze, and Ondřej Malina

ABSTRACT: The 1:1:1 reaction of $DyCl_3 \cdot 6H_2O$, $K_3[Co(CN)_6]$ and $bpyO_2$ in H_2O has provided access to a complex with formula $[DyCo(CN)_6(bpyO_2)_2(H_2O)_3] \cdot 4H_2O$ (**1**) in a very good yield, while $[DyFe(CN)_6(bpyO_2)_2(H_2O)_3] \cdot 4H_2O$ (**2**) was also precipitated (also in a high yield) using $K_3[Fe(CN)_6]$ instead of $K_3[Co(CN)_6]$. Their structures have been determined by single crystal X ray crystallography and characterized based on elemental analyses and IR spectra. Combined direct current (dc) and alternating current (ac) magnetic susceptibility revealed slow magnetic relaxation upon application of a dc field. μ SQUID measurements and CASSCF calculations revealed high temperature relaxation dynamics for both compounds. Low temperature magnetic studies show the relaxation characteristics for **1**, while for compound **2** the dynamics corresponds to an antiferromagnetically coupled Dy···Fe pair. High resolution optical studies have been carried out to investigate the performance of compounds **1** and **2** as luminescence thermometers. For **1**, a maximum thermal sensitivity of 1.84% K^{-1} at 70 K has been calculated, which is higher than the acceptable sensitivity boundary of 1% K^{-1} for high performance luminescence thermometers in a broad range of temperature between 40 and 140 K. Further optical studies focused on the chromaticity diagram of compound **1** revealed a temperature shift from warm white (3200 K) at 10 K toward a more natural white color near 4000 K at room temperature.

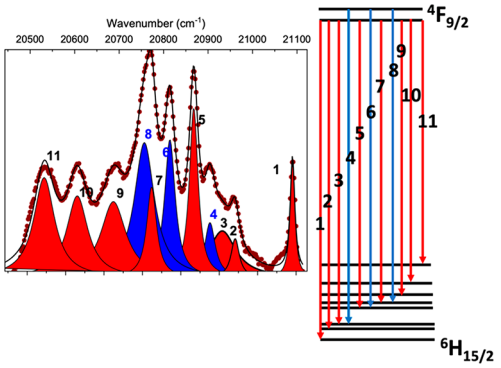

INTRODUCTION

Multifunctional materials currently attract the intense interest of scientists working in several fields of materials science, chemistry, and physics.[1−7] Except for the purpose of obtaining fundamental knowledge, researchers pursue the implementation of such material in practical applications. Such materials can be used to construct smart devices consisting of composites of different functional units or containing homogeneous matter in which properties have been introduced at the molecular level. Incorporating two or even three different physical properties into a single phase material allows the observation of cooperative effects[3] or the effect of one functionality onto another.[4,5] If the properties are not coupled, then applications may arise from the realization of the properties under the same operational conditions.[6,7]

Lanthanide(III) [Ln(III)] based complexes (either homometallic or heterometallic) are at the heart of the research efforts in molecular materials,[8,9] finding applications in light emitting diodes (LEDs), display devices, optical sensing, and bioimaging. Heterocyclic ligands, especially the derivatives bearing *N* oxide functions, are particularly stable and can be efficient sensitizers for Ln(III) emission upon UV radiation.[10] A useful derivative related to the present work is 2,2′ bipyridine *N*,*N*′ dioxide ($bpyO_2$).[10−12] For example, a detailed comparative study was carried out by Eliseeva, Bünzli, and co workers to investigate the exact influence of the introduction of $bpyO_2$ in the inner coordination sphere of Eu(III) upon replacement of the two aqua ligands in $[Eu(hfac)_3(H_2O)_2]$, where $hfac^-$ is the hexafluoroacetylacetonate(−1) ligand.[12] This leads to a 15 fold increase in the overall quantum yield of $[Eu(hfac)_3(bpyO)_2]$. This impressive improvement originates from (i) a better sensitization efficiency, the ancillary $bpyO_2$ ligand being responsible for 3/4 of the energy transfer, (ii) elimination of nonradiative deactivation pathways through harmonics of O−H vibrations, and (iii) reduction in the

radiative lifetime. The latter influence is rarely documented, but it accounts for an increase of ~25% in the intrinsic quantum yield of $[Eu(hfac)_3(bpyO)_2]$.

The incorporation of both magnetic and optical properties in a coordination complex is a modern research theme in inorganic chemistry.[13] Luminescent SMMs are of great importance for the detailed investigation of the mechanisms underlying the magnetization relaxation in mononuclear Ln^{III} complexes;[14] photoluminescence studies can, in principle, allow the spectroscopic determination of the Stark sublevels of some Ln(III) ions and compare them with those derived from magnetic studies.[15−18] Another emerging research area which takes advantage of the combination of SMM and luminescence properties in Ln(III) complexes is SMM luminescence thermometry.[19] A great challenge, however, remains the monitoring of the temperature changes in real time during the operation of the electronic device; temperature changes are a crucial factor in the operation of SMMs, because they are related to the ability of molecules to remain magnetized and therefore behave as magnetic memories. Since conventional contact thermometers cannot be used for this goal because they perturb the system,[20] a promising solution to the problem is to take advantage of the temperature dependence of the Ln(III) ions emission.[19] It is thus evident that the marriage of SMM and luminescence properties in the same complex will help researchers to understand the principles of heat generation in devices and monitor the temperature during the operation of future SMM based devices. The ideal situation is an overlap in the working temperature of the two properties. This gives the opportunity for contactless temperature monitoring of the SMM operation in real time in a low temperature range in which spectral changes and SMM behavior is observed. Since some thermally activated mechanisms of magnetization relaxation occur at the level of individual Ln(III) SMM affecting the luminescence of a complex in different temperature ranges, expansion of the thermal probing capabilities of the system at higher temper atures (even above room temperature) is also possible.[19] Thus, the broad temperature range encompasses the superparamag netic SMM range (at low temperatures) to the application range of electronic devices (near room temperature). Another important feature is that the luminescent thermometer properties are retained under applied magnetic fields, and this opens the avenue for optomagnetic investigations on next generation devices.[21]

The central goal of this work was to contribute into the phenomenon of SMM luminescent thermometry based on heterometallic 3d/4f metal complexes;[22−26] For the synthesis of 3d/Ln(III) metal complexes we decided to use the CN^-/$bpyO_2$ ligand "blend". Anticipating that $bpyO_2$ would chelate to Dy(III), we predicted that this ligand might be an efficient sensitizer for Dy(III) emission (*vide supra*), ensuring interesting optical properties.[10−12] However, the bridging cyano ion is a popular ligand for the synthesis of heterometallic 3d/*n*d and 3d/4f metal SMMs.[2,26−35] Its tendency for bridging only two metal ions, one at each end, to afford a linear bridging motif is well documented. As a source of the 3d metal ion, we used the octahedral $[M(CN)_6]^{3-}$ anions (M(III) = Co and Fe). The diamagnetic $[Co(CN)_6]^{3-}$ ions are able to magnetically separate[35] the Dy(III) ions (in the case of complexes containing more than one Dy(III) center) enhancing their emission or to strengthen the single ion properties of Dy(III) in complexes with one such center improving their SMM (SIM) performance. In addition, the bridging $[Co(CN)_6]^{3-}$ linker can be red emissive, providing a chance for energy transfer to the 4f metal ions,[35] and there have been reports of emissive Dy(III) SMMs sensitized by this diamagnetic linker.[34,35] The paramagnetic $[Fe(CN)_6]^{3-}$ (S = 1/2) ion was expected to introduce Fe···Dy(III) exchange interactions affecting significantly the magnetic properties of the products (e.g., the relaxation pathways in the case of SMMs) and the Dy(III) emission characteristics. This work describes our results in topics related to the above mentioned points.

RESULTS AND DISCUSSION

Synthesis and IR Spectra. Once we had selected to study the Dy(III)/M(III)/CN^-/$bpyO_2$ (M = Co and Fe) reaction

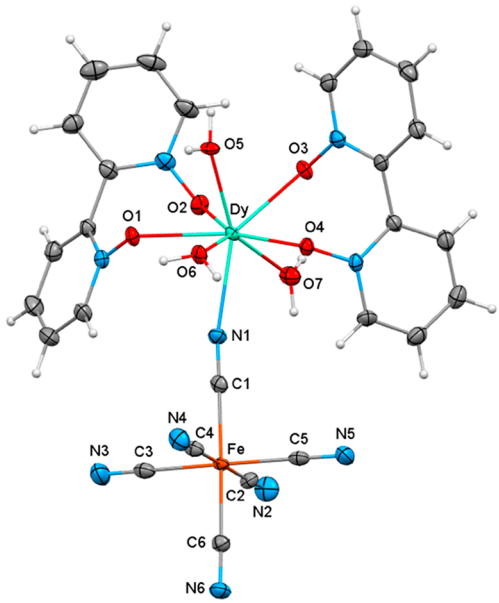

Figure 1. Partially labeled plot of the structure of the molecule $[DyFe(CN)_6(bpyO_2)_2(H_2O)_3]$ in the crystal of **2**·$4H_2O$.

systems (for reasons outlined in the Introduction), we carried out a literature survey which revealed that complexes $[GdFe(CN)_6(bpyO_2)_2(H_2O)_3]\cdot 4H_2O$[36] and $[SmFe(CN)_6(bpyO_2)_2(H_2O)_3]\cdot 4H_2O$[37] had been prepared and structurally characterized. In the former, the intramolecular Gd(III)···Fe(III) exchange interaction is weakly ferromagnetic, while the latter exhibits weak green, Sm(III) based lumines cence at room temperature. No Dy(III)/ Co(III)/CN^-/$bpyO_2$ complexes existed in the literature. Thus, we decided to pursue studies using Dy(III) and Co(III) or Fe(III) sources.

The 1:1:1 reaction of $DyCl_3\cdot 6H_2O$, $K_3[Co(CN)_6]$ and $bpyO_2$ in H_2O resulted in a yellow solution from which pale yellow crystals of $[DyCo(CN)_6(bpyO_2)_2(H_2O)_3]\cdot 4H_2O$ (**1**) were subsequently isolated in a very good yield (~75%). Crystals of $[DyFe(CN)_6(bpyO_2)_2(H_2O)_3]\cdot 4H_2O$ (**2**) were precipitated (also in a high yield) using $K_3[Fe(CN)_6]$ instead of $K_3[Co(CN)_6]$.

In the IR spectra of the complexes (Figure S1), the strong bands centered at ~3350 and ~3125 cm^{-1} are due to the ν(OH) vibration of the lattice and coordinated H_2O molecules, respectively.[38] The broad character of the bands suggests the involvement of the H_2O molecules in H bonding interactions. The δ(OH) vibration of H_2O appears at ~1635

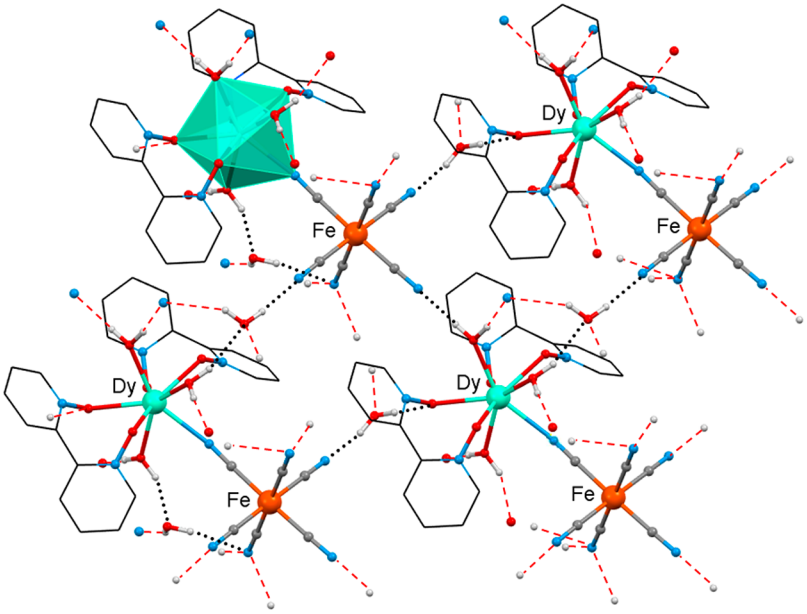

Figure 2. Layer of the 3D architecture of complex **2** parallel to the *ab* plane. The O−H···O/N intermolecular H bonds connecting the molecules in the layer are shown in dotted black lines; hanging contacts to atoms on adjacent layers are drawn with dashed red lines. Only contact H atoms are drawn.

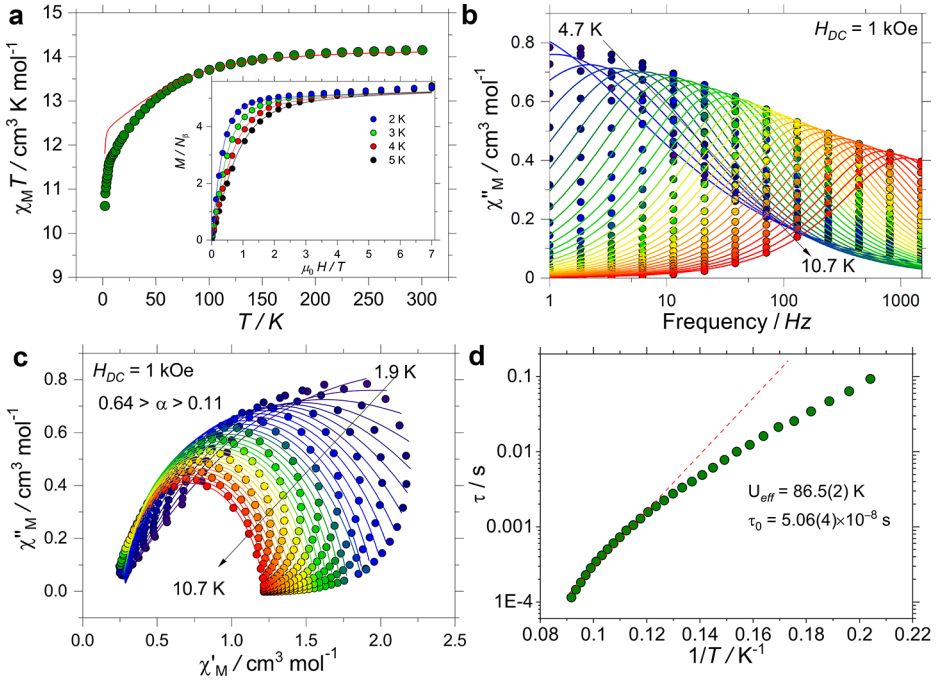

Figure 3. (a) Experimental $\chi_M T(T)$ H_{dc} = 1 kOe and the $M(H)$ between 2 and 5 K (inset) for complex **1**. The solid lines corresponds to the simulated $\chi_M T(T)$ and $M(H)$ traces employing the crystal field parameters obtained from CASSCF calculations; (b) $\chi_M''(\nu)$ at zero dc field. (c) Cole plots ($\chi_M''(\nu)$ vs $\chi_M'(\nu)$) showing a single relaxation process. (d) τ vs $1/T$ plots of ac data at zero field and Arrhenius treatment for ac data. Solid lines in panel (b) and (c) are the fit to a single Debye process.

cm^{-1}. The bands in the 1560−1420 cm^{-1} region are assigned to the stretching vibrations of the heterocyclic rings of coordinated bpyO$_2$;[12] these modes are slightly shifted compared to those of free bpyO$_2$. The strong band at 1254 cm^{-1} in the spectrum of the free ligand has been assigned[12] to the ν(N−O) vibration; this bands shifted to ∼1215 cm^{-1} in the spectra of the complexes due to the O,O′ coordination of the ligand. The strong bands at 2128 cm^{-1} in the spectra of **1** is assigned[39] to the ν(C≡N) mode of the terminal C bonded cyano ligands. The corresponding band in **2** is located at 2113 cm^{-1}. The ν(C≡N) mode of free CN$^-$ appears at 2080 cm^{-1} in ionic salts, such as NaCN. The CN$^-$ ion acts as a σ donor by donating electrons to the metal center and as a π acceptor by accepting electrons from the metal. σ Donation tends to raise the ν(C≡N) since electrons are removed from the 2σ orbital, which is weakly antibonding, whereas π back bonding tends to decrease the ν(C≡N) because electrons enter into the antibonding 2pπ* orbitals. Since CN$^-$ is a very good σ

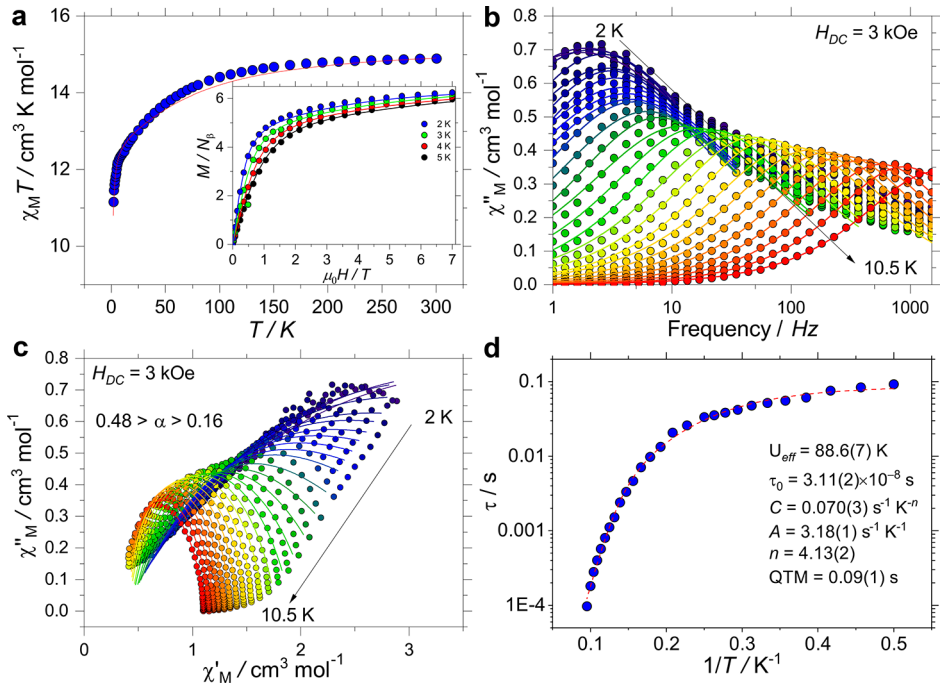

Figure 4. (a) Experimental $\chi_M T(T)$ H_{dc} = 3 kOe and the $M(H)$ between 2 and 5 K (inset) for complex **2**. The solid lines corresponds to the simulated $\chi_M T(T)$ and $M(H)$ traces employing the crystal field parameters obtained from CASSCF calculations for Dy(III) and g values for Fe(III) leading to a $J = -1.35$ cm^{-1} employing a $-2J$ Hamiltonian. (b) $\chi_M''(\nu)$ at zero dc field; (c) Cole plots ($\chi_M''(\nu)$ vs $\chi_M'(\nu)$) showing a single relaxation process. Solid lines in panel (b) and (c) are the fit to a single Debye process. (d) Experimental τ vs $1/T$ plots data (symbols) and fit employing $\tau^{-1} = \tau_0^{-1} \exp\left(-\frac{U_{eff}}{T}\right) + CT^n + AT$ (solid line) and parameters described in the text and inset of figure.

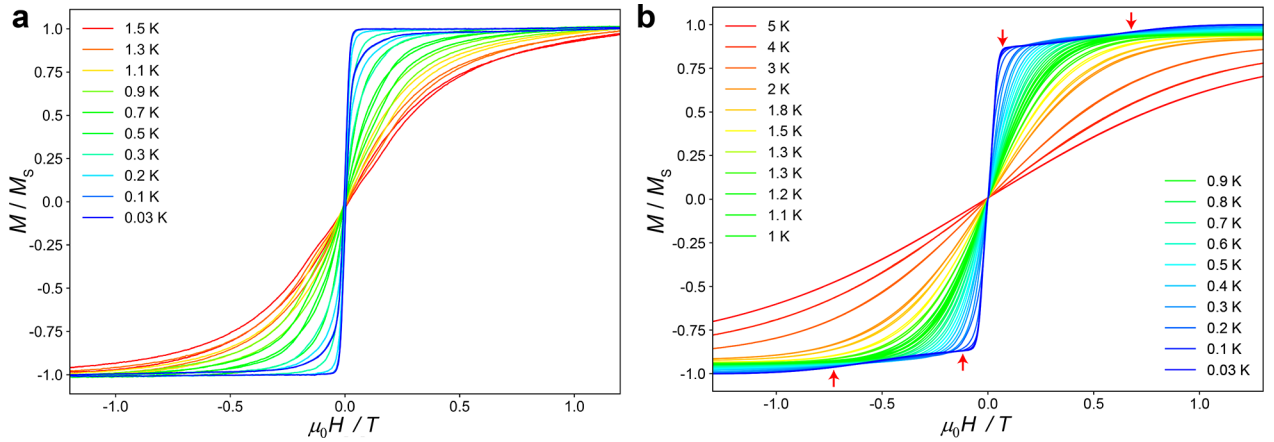

Figure 5. μ SQUID loops obtained from single crystal measurements of compounds **1** (a) and **2** (b). The red arrows in panel b indicate the range in which the broad inflection, which hints to the possibility of antiferromagnetic interactions, is observed.

donor and a rather poor π acceptor, the ν(C≡N) wave numbers of complexes containing C bonded terminal cyano ligands are generally higher than the value of free CN^-.[39] The higher wavenumber for {DyCo} complex **1** is in agreement with literature data[39,40] according to which the ν(C≡N) wavenumber increases as the number of d electrons in the t_{2g} level increases in low spin octahedral cyano complexes (this number is 6 for **1** and 5 for **2**). Since one of the cyano groups in both complexes is bridging (M(III)−C≡N−Ln(III), *vide infra*), we would expect two ν(C≡N) bands, with the band for the bridging cyano group being at a higher wavenumber than for the terminal cyano groups.[39] This, indeed, is observed in the spectra, and the bands at 2140 cm^{-1} (for **1**) and 2130 cm^{-1} (for **2**) are assigned to the ν(C≡N) mode of the bridging cyano group.

Description of Structures. The crystal structures of **1** and **2** were determined by single crystal X ray crystallography (see the Experimental Section in the Supporting Information and Table S1). Various structural plots are shown in Figures 1, 2, and S2. Selected interatomic distances and angles are listed in Table S2. The two complexes are isomorphous since (i) they both crystallize in the same triclinic $P1$ space group and have quite similar cell dimensions and (ii) the types and the positions of atoms in both structures are the same except for the replacement of the Co(III) center in **1** with the Fe(III) atom in **2**. Thus, a general description of the structures is given below. The same numbering scheme has been assigned to the

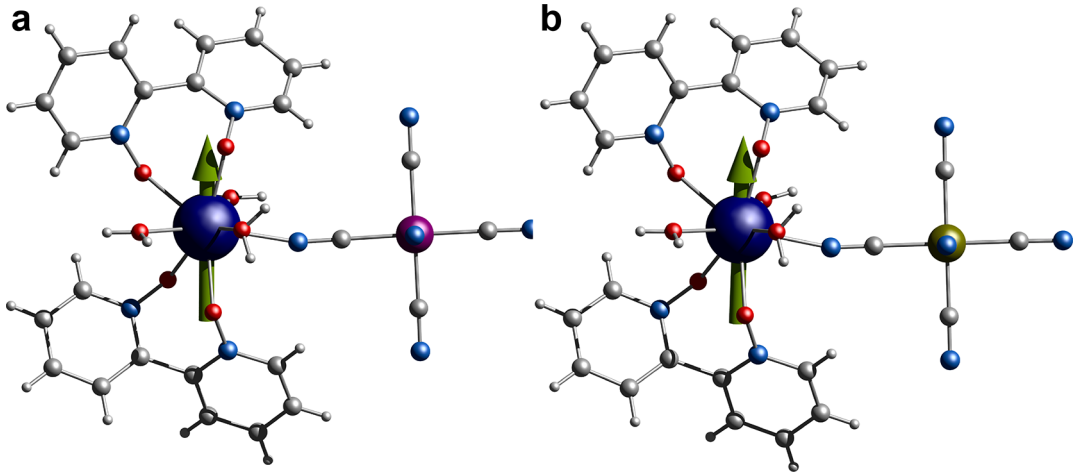

Figure 6. Direction of the principal axis of the *g* tensor in the ground Kramer doublet of compounds **1** (a) and **2** (b) showing the similar magnetic axis for both complexes. Color code: Dy, blue; C, black; H, light gray; N, pale blue; O, red; Fe, pale green; and Fe, purple.

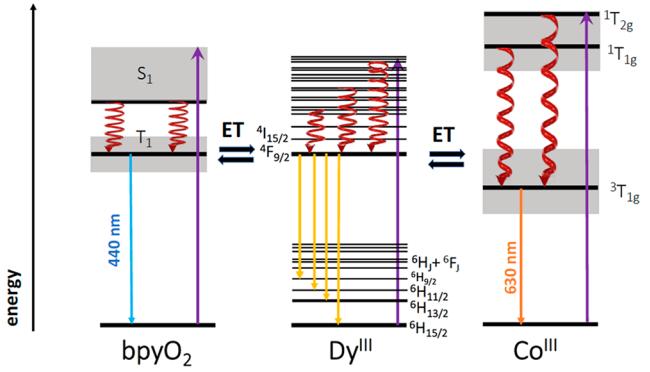

Figure 7. Schematic energy diagram of the multiple emissive centers of **1**. The vertical arrows represent, depending on the color and the direction, (a) emission peaks which contribute to the luminescence of **1** (colored downward), (b) UV excitation (violet upward), (c) nonradiative relaxation (wine red wavy lines), and (d) energy transfer process (black horizontal).

ligands' (CN^-, $bpyO_2$, and H_2O) and lattice H_2O atoms of the three compounds.

The crystal structures consist of heterodinuclear $[DyM(CN)_6(bpyO_2)_2(H_2O)_3]$ (M = Co and Fe) molecules and lattice solvent H_2O molecules in an 1:4 ratio. In the dinuclear molecules, the Ln(III) and M(III) centers are bridged by a cyano group (Ln−N≡C−M). Two O,O′ bidentate chelating $bpyO_2$ molecules and three aqua ligands complete the 8 coordination at Ln^{III}, while five terminal C bonded cyano groups complete the coordination sphere of the transition metal ion. Thus, the coordination spheres are $\{Ln^{III}O_7N\}$ and $\{M^{III}C_6\}$. The Co^{III}−C [1.886(4)−1.915(5) Å] and Fe^{III}−C [1.932(4)−1.962(4) Å] bond lengths are indicative of low spin 6 coordinate metal ions.[34,35] The Dy^{III}−O/N bond distances [2.287(3)−2.460(4) Å for **1** and 2.296(3)−2.469(3) Å for **2**] are typical for complexes containing 8 coordinate Dy^{III} ions.[11,34,35] The carbon nitrogen bond lengths of the cyano groups are in the ranges of 1.136(5)−1.150(6) Å and 1.143(6)−1.155(6) Å for **1** and **2**, respectively. Each $bpyO_2$ ligand forms a skewed 7 membered chelating ring with the Ln^{III} center. The nitrogen−oxygen bond lengths of the pyridine−*N* oxide moieties of the $bpyO_2$ ligands span the ranges of 1.323(4)−1.334(4) Å in **1** and 1.317(5)−1.329(4) Å in **2**. The corresponding distance in the crystal structure of the free $bpyO_2$ molecule is 1.302(2) Å.[41,42] The slight lengthening of this bond in the complexes can be attributed to coordination.

The coordination geometries of the M(III) ions in the complexes are octahedral, with the *trans* C−M^{III}−C angles in the ranges of 177.4(4)−179.0(4)° for **1** and 177.7(3)−178.9(4)° for **2**. To evaluate the coordination polyhedron defined by the donor atoms around the Ln^{III} center in the three isomorphous complexes, the experimental data were compared to the theoretical values for the common polyhedral with eight vertices using SHAPE.[43] The so named Continuous Shape Measures (CShM) approach allows us to numerically estimate how far a real coordination sphere of a metal center deviates from an ideal polyhedron. Of the accessible 8 coordinate polyhedral for metal ions, the triangular dodecahedron is the most appropriate for the description of the 8 donor atoms around Dy^{III} for **1** and **2** (Table S3). The same conclusion is also reached applying the angular criteria proposed by Kepert.[44] The Co−C≡N [177.4(4)−179.5(5)°] and Fe−C≡N [177.7(3)−178.9(4)°] bond angles do not deviate from linearity. The two $bpyO_2$ ligands create a steric hindrance on Ln^{III} leading to a significant bending of the intermetallic cyano bridge[34] as revealed by the Ln−N≡C angle of ∼165.5°. The dihedral angles between the heterocyclic rings are 62.0(2) and 58.6(1)° for **1** and 62.7(1) and 58.6(1)° for **2**, smaller than the corresponding angle in the uncoordinated $bpyO_2$ molecule (∼67.7°).[41]

The dinuclear molecules for all three complexes are arranged in layers parallel to the *ab* plane, and the interlayer space is filled by the lattice solvent (crystallization) H_2O molecules (Figure 2). A plethora of intermolecular H bonds (Tables S4 and S5), involving the five terminal cyano groups of the $\{M^{III}(CN)_6\}^{3-}$ moieties and all the coordinated and lattice H_2O molecules, firmly link the dinuclear molecules within each layer as well as between adjacent layers toward a robust 3D architecture. Each coordinated H_2O molecule participates in two H bonds with the O atom acting as donor, whereas the more versatile lattice H_2O molecules form up to four H bonds with their O atoms behaving as both donors and acceptors. The crystal structures are further stabilized by $\pi\cdots\pi$ stacking interactions formed between molecules that belong to adjacent

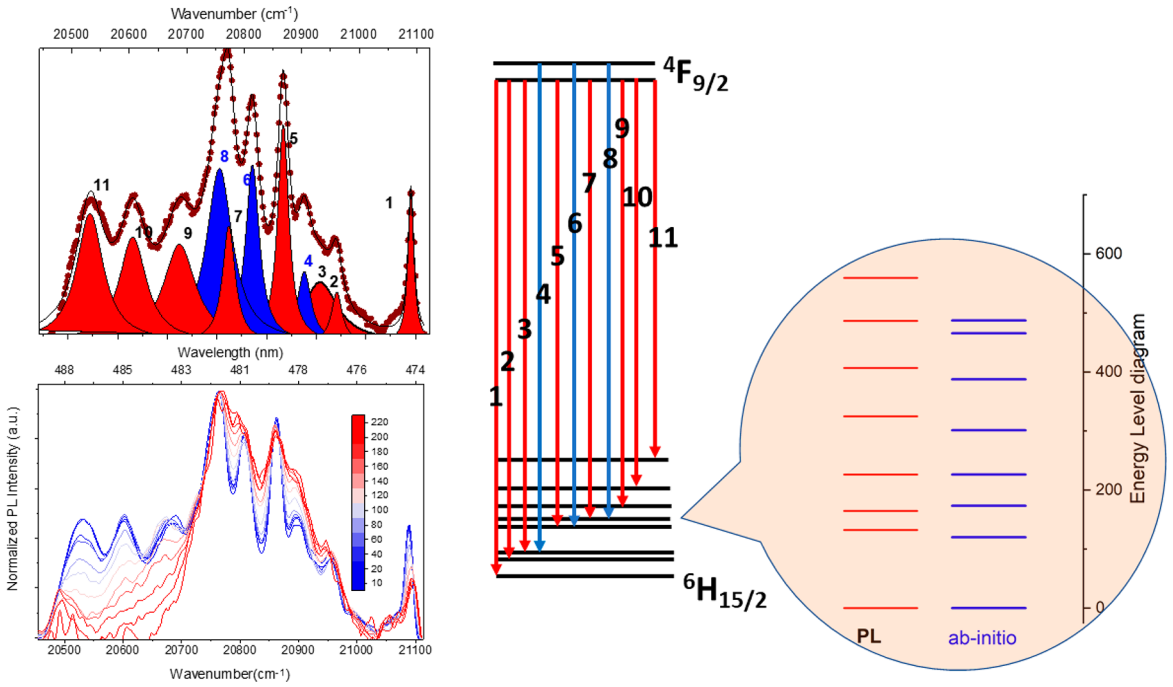

Figure 8. (top left) High resolution emission spectrum of the $^4F_{9/2} \rightarrow {}^6H_{15/2}$ transition obtained under UV excitation (375 nm) at 10 K (wine solid spheres represent the experimental PL data and the black solid line the fitting results). The deconvolution of the spectrum reveals eight peaks (red colored) in accordance to the ab initio calculations and 3 components (blue colored) arising from electronic transition from the second m_J level of the excited $^4F_{9/2}$ Stark multiplet (hot bands). (bottom left) Temperature dependent emission spectrum of the $^4F_{9/2} \rightarrow {}^6H_{15/2}$ transition from 10 to 220 K revealing the existence of hot bands in the area 20 700−20 950 cm^{-1}. (middle) Energy spectrum according to the deconvolution of the $^4F_{9/2} \rightarrow {}^6H_{15/2}$ transition. The numbering (1−11) and the color code is according to the emission spectrum, assigning the transition coming from the first (0−0 red colored transitions) and the second (1−0 blue colored transitions) Stark sublevels of the $^4F_{9/2}$. (right) Comparison of the position of the Stark sublevels of the $^6H_{15/2}$ Dy^{III} levels based on the PL studies and ab initio calculations (see also Table S8).

layers; there are two such interactions per dinuclear molecule with centroid−centroid distances of ∼3.80 and ∼3.85 Å.

Compound **1** is the first structurally characterized heterometallic $\{Co^{III}Ln^{III}\}$ complex bearing both cyano and $bpyO_2$ ligands, while **2**·$4H_2O$ is isomorphous to the previously reported $[LnFe^{III}(CN)_6(bpyO_2)_2(H_2O)_3]$ (Ln = Sm and Gd)[36,37] complexes. Complexes **1** and **2** join a small family of homometallic[10,12,45] or heterometallic[11,36,37] complexes containing $bpyO_2$ molecules coordinated to Ln^{III} centers.

Static Magnetic Properties. The $\chi_M T(T)$ static magnetic susceptibility for **1** and **2** in an applied magnetic field of H_{dc} = 1 kOe (χ_M is the molar magnetic susceptibility, where "dc" denotes direct current), are shown in Figures 3a and 4a. For the case of **1**, the room temperature value of $\chi_M T$ is 14.1 cm^3 mol^{-1} K as expected for an isolated Dy(III) ion, while for the case of **2**, the $\chi_M T$ value is 14.9 cm^3 mol^{-1} K, slightly higher than the expected for two noninteracting Dy(III) and an isotropic spin half for a low spin Fe(III) (i.e., 14.5 cm^3 mol^{-1} K). Upon cooling, the $\chi_M T(T)$ profile remains practically constant down to ca. 100 K for both complexes, at which point it starts decreasing (Figure 3). The downturn observed in the $\chi_M T(T)$ data for both complexes can be attributed to the depopulation of crystal field levels. For the case of **2**, the downturn can also be ascribed to antiferromagnetic interactions operating between the Dy(III) and the Fe(III) ions. The molar magnetization M as a function of the applied magnetic field of **1** and **2** is shown in the insets of Figure 3a and 4a, respectively. For the case of **1**, the saturation value of M at 7 T is 5.4 μ_B, suggesting a nearly pure $m_J = \pm 15/2$ state, with negligible Dy−Dy interactions due to the diamagnetic spacer anion $[Co(CN)_6]^{3-}$. The saturation magnetization value for the case of **2** is 6.1 μ_B confirming the presence of the spins of the Dy(III) ion with a nearly pure $m_J = \pm 15/2$ state and a Fe^{III} ion with $S = 1/2$, $M_{tot} = M_{Dy} + M_{Fe} \sim (5.1 + 1.0)\ \mu_B = 6.1\ \mu_B$.

Dynamic Magnetic Properties. The dynamic behavior of all two complexes was probed via magnetic susceptibility alternating current (ac) studies employing an oscillating field of 3.5 Oe. A clear SMM behavior was observed for complexes **1** and **2** upon application of a direct current (dc) field. As observed in Figure 3b, **1** shows a frequency dependent out of phase magnetic susceptibility $\chi_M''(\nu)$, with a maximum at temperatures between 4.7−10.7 K with an applied field of 1 kOe. The $\chi_M''(\nu)$ maximum shifts with increasing temperatures at temperature, indicating the temperature dependent regime. $\tau(T)$ can also be extracted by fitting the Cole−Cole plot to a single process between 4.7 and 10.7 K (Figure 3c). The energy barrier can be obtained from the linear portion of $\tau(T)$, leading to U_{eff} = 86.5(2) K and $\tau_0 = 1.05(2) \times 10^{-6}$ s, and $0.53(3) > \alpha > 0.12(1)$ indicating a relatively wide distribution of processes (Figure 3d) and fast relaxation.

The temperature and frequency dependent out of phase magnetic susceptibilities for complex **2** ($\chi_M''(T)$ and $\chi_M''(\nu)$, respectively) are shown in Figure 4b,c, revealing also a maximum at temperatures between 2−10.5 K with an applied field of 3 kOe. $\tau(T)$ can be extracted by fitting the $\chi_M''(\nu)$ data to a single process between 2 and 10.7 K leading to $0.48(2) > \alpha > 0.16(1)$, indicating a similar distribution of relaxation processes in comparison to **1**. As described, **1** shows SMM signatures under a 1 kG applied dc field, while to reveal the SMM characteristic in **2**, a larger field of 3 kG is required. Furthermore, for **1** the maximum of $\chi_M''(\nu)$ lies below 1 Hz,

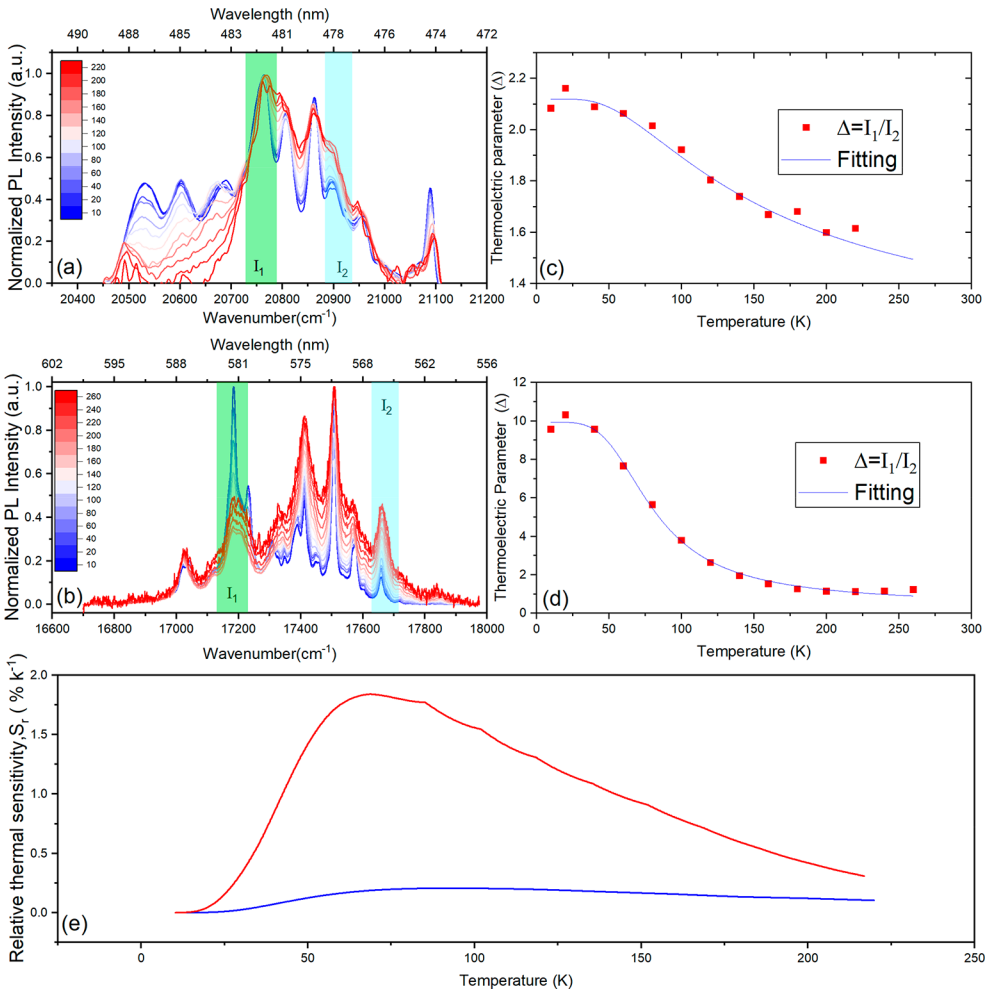

Figure 9. (a) Temperature dependence spectra of the $^4F_{9/2} \rightarrow {}^6H_{15/2}$ transition and (b) the $4F_{9/2} \rightarrow {}^6H_{13/2}$ transition band for **1** with the selected integrated areas highlighted with green (I_1) and blue (I_2) areas. (c and d) Temperature dependence of the thermometric parameter obtained in (a) and (b), respectively, and their fitting curve via a Mott−Seitz model. (e) Thermal relative sensitivity obtained for approaches 1 (blue line) and 2 (red line).

being maximally temperature dependent from 4.7 to 10.7 K. In contrast, the maximum in $\chi_M''(\nu)$ is already observed at 2 K at 2.5 Hz, which stays practically constant up to 4.4 K when it becomes temperature dependent. Moreover, the more pronounced deviation of $\ln(\tau)$ as a function of inverse temperature from linearity below 5 K for compound **2** as well as the negligible χ_M'' signal at zero dc external field provides strong evidence for additional relaxation processes. The relaxation data for **2** can be fitted considering the Orbach, Raman, Direct, and quantum tunnelling of the magnetization processes employing $\tau^{-1} = \tau_0^{-1} \exp\left(-\frac{U_{eff}}{T}\right) + CT^n + AT$. The best fit yields values of $\tau(T)$ $U_{eff} = 88.6(7)$ K, $\tau_0 = 3.11(2) \times 10^{-8}$ s, $C = 007(3)$ s^{-1} K^{-n}, $A = 3.18(1)$ s^{-1} K^{-1}, $n = 4.13(2)$, and $\tau_{QTM} = 0.09(1)$ s (Figure 4d). Attempts to fit the $\tau(T)$ data for **1** employing the Orbach, Raman, or Direct relaxation process did not result in sensible values. Comparison of the U_{eff} for both complexes clearly indicates that the thermally active regime in both cases leads to similar barriers (cf. 86.5(2) K for **1** and 88.6(7) K for **2**), while larger deviation for the relaxation dynamics is observed at lower temperatures.

***μ*-SQUID.** To confirm the SMM characteristics observed in the ac studies, μ SQUID loops were collected on single crystals of compounds **1** and **2** with the field aligned along the easy axis of the crystal. The resulting loops show the typical, temperature and sweep dependent butterfly like loops commonly observed in lanthanide based SMMs (Figure 5). For **1**, a small opening is observed, while for **2** the loops are practically closed, indicating faster relaxation in **2** than in **1**. This is consistent with the ac susceptibility data, which requires a larger field for **2** to obtain the lowest relaxation characteristics of the complex. Additionally, for **2** a very broad inflection is present in the ranges between ca. ±0.1 and ±0.8 T, indicative of antiferromagnetic interactions between the Fe(III) spin, expectedly, $S = 1/2$ for strong field configuration ion $[Fe(CN)_6]^{3-}$, and the electronic spin for Dy(III) (Figure 5b). Unfortunately, due to the broad profile it is not possible to directly extract the interaction between the metal ions employing the mean field approximation.

Theoretical Studies. To gain further insight into the magnetization blocking of compounds **1** and **2**, *ab initio* calculations were carried out with the CASSCF/SO RASSI/SINGLE ANISO approach implemented in the Molcas 8.2 program package. For this purpose, the crystal structures of **1** and **2** were employed without further optimizations, with the atoms being described using standard basis sets from the ANO RCC library available in Molcas.[46−48] For the calculation of the magnetic properties of **2**, the Fe(III) ion was substituted

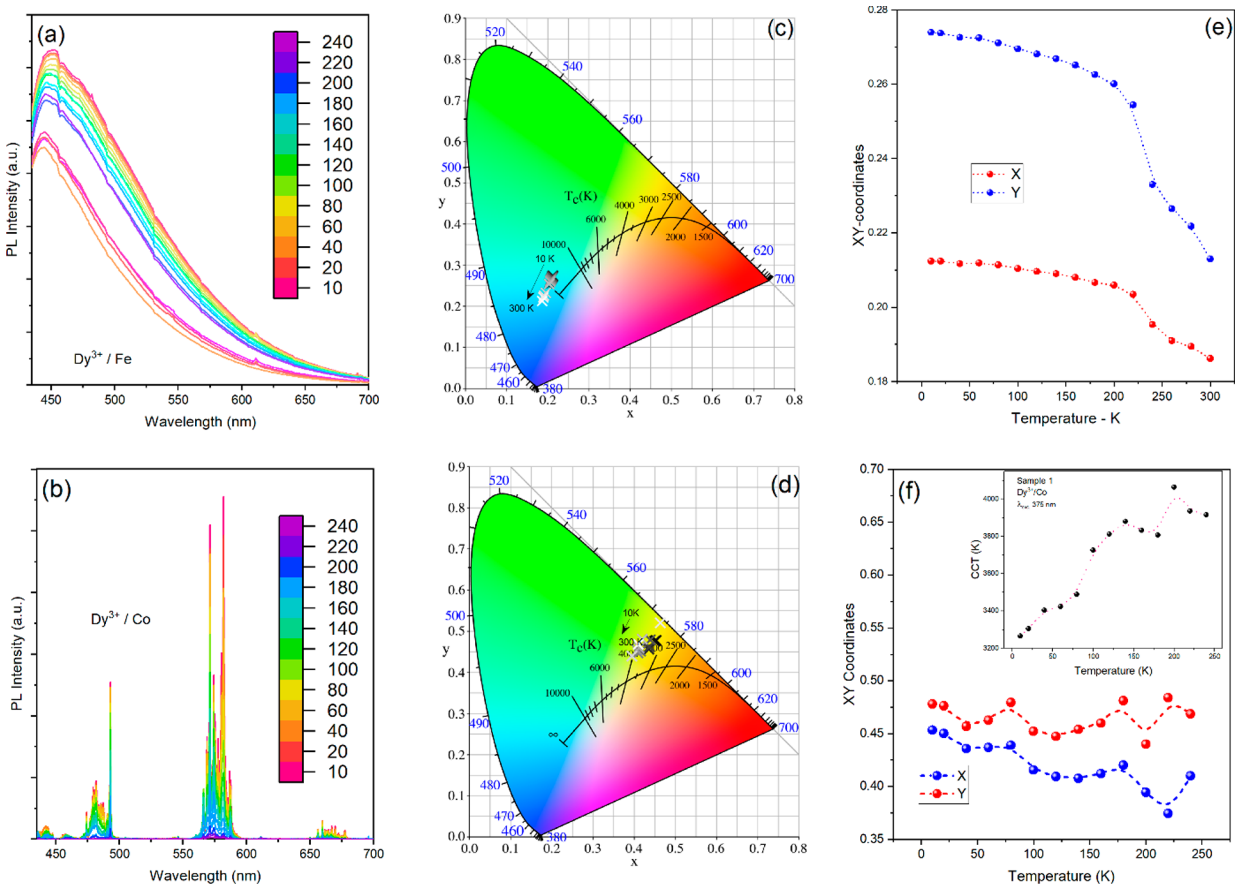

Figure 10. (a and b) Temperature dependence spectra of **2** and **1** respectively. (c) and (d) Respective emission colors appeared in the CIE 1931 chromaticity diagrams for **2** and **1** respectively. Their (x, y) coordinates are presented in (e) and (f), for **2** and **1** respectively, while the inset graph in (f), shows the correlated color temperature (CCT) for **1** over temperature.

Table 1. Thermoelectric Parameter (Δ) Fitting Parameters

band transition	Δ_0	α_1	α_2	E_1 (meV)	E_2 (meV)
480 nm	2.1	0.8		17.5	
560 nm	9.9	1.6	31	13.8	27.2

by Co(III) atom. For the dysprosium ions, a basis set of VTZP quality was employed, while VDZP quality was used for atoms directly bound to the Dy(III) ions. VDZ quality was used for the remaining atoms. The molecular orbitals (MOs) were optimized in state averaged CASSCF calculations. For this, the active space was defined by the nine 4f electrons in the seven 4f orbitals of Dy(III). Three calculations were carried out independently for each possible spin state, where 21 roots were included for S = 5/2, 224 roots were included for S = 3/2, and 490 roots were for S = 1/2 (RASSCF routine). The wave functions obtained from these CASSCF calculations were posteriorly mixed by spin−orbit coupling, where all 21 S = 5/2 states, 128 of the S = 3/2 states, and 130 of the S = 1/2 states were included (RASSI routine). The crystal field decomposition of the ground J = 15/2 multiplet of the $^6H_{15/2}$ term was executed with the SINGLE_ANISO module.[46]

The energies of low lying Kramers doublets and the main components of the g tensor of the Dy(III) ion for **1** and **2** are shown in Table S6 and S7 respectively. The main magnetic axis (z) on the Dy ion is indicated in Figure 6 by the green arrow, and it demonstrates that the presence of the $[Co(CN)_6]^{3-}$ or $[Fe(CN)_6]^{3-}$ does not influences the magnetic anisotropy axes of the Dy(III) ion. In both cases, the ground Kramer doublet state is strongly axial, with g values close to $g_x = g_y = 0.0$ and $g_z = 20$. The first excited state lies between 113 and 120 cm^{-1}, and the second excited state is between 165 and 173 cm^{-1}. The magnitude of the energy barriers obtained for **1** and **2** are lower than the separation between the first excited state and the ground state obtained from CASSCF calculation, which indicates that under barrier processes are active in both complexes.[49]

By employing the crystal field parameters obtained from CASSCF calculations, it is possible to observe a rather good agreement between the calculated and experimental $\chi_M T(T)$ and $M(H)$ data for **1**. Some differences between the calculated and experimental $\chi_M T(T)$ are observed at low temperatures, which might arise from intermolecular interactions not accounted for in theoretical study. The presence of the paramagnetic Fe(III) ions requires further investigation of the magnetic characteristic of the $[Fe(CN)_6]^{3-}$ unit. To estimate the interaction between Fe(III) and Dy(III) in **2**, CASSCF calculations were also carried out by substituting Dy(III) in **2** by Y(III), while keeping Fe(III) as the paramagnetic species. The results show an isolated doublet state with g values g_x = 3.00, g_y = 2.40, and g_z = 0.85, consistent with the low spin characteristics of similar complexes containing the $[Fe(CN)_6]^{3-}$ unit.[50−52] By employing the crystal field parameters for Dy(III) in **2** and the g values for the S = 1/2 state of the $[Fe(CN)_6]^{3-}$ unit, it is possible to simulate the experimental $\chi_M T(T)$ and $M(H)$ data for **1**, leading to a an antiferromag

netic exchange interaction operating between the Fe(III)···Dy(IIII) ion of $J = -1.35$ cm^{-1} (for a $-2J$ Hamiltonian), consistent with the inflection observed in the μ SQUID data.

With a clearer electronic structure picture, it is possible to rationalize the dynamic magnetic behavior observed for **1** and **2**. As observed in the dynamic magnetic data, **1** is an SMM in field; that is, it requires the application of an H_{dc} = 1 kG field to decrease the fast relaxation, which precludes the observation of SMMs signature at zero field. **2** is also an SMM in field, however it is characterized as a coupled system where the spin of the Fe(III) interacts with the electronic spin of Dy(III) by an antiferromagnetic interaction, which in turn enhances the relaxation characteristic of the complex. As a result, a larger H_{dc} (3 kG), acting as a decoupling field, is required to drive the system out of the fast relaxation region, revealing the SMM characteristics of the complex. Once the field has been applied, the system is far from the fast relaxation region, and the relaxation dynamics of **1** are consequently similar to the dynamics of **2**, as observed in the similar U_{eff} obtained, in the high temperature region. In contrast, the relaxation characteristics for both complexes is different at lower temperatures, as observed in the plot of $\ln(\tau)$ versus $1/T$: While for **1** the relaxation depends entirely on the magnetic characteristic of the Dy(III) ion, in **2**, the interaction between the Dy(III) and Fe(III) creates further relaxation pathways, which are more evident at lower temperatures due to the small interaction between the spin pair. This is evidence in the different $\ln(\tau)$ versus $1/T$ profiles at low temperatures observed for **1** and **2** as well in the μ SQUID hysteresis loops.

Optical Studies-Luminescence Thermometry. The effect of the crystal field on the ground state multiplets ^6H_J of Dy(III) is reflected in the high resolution emission spectrum of **1** upon UV excitation (375 nm) where four characteristic electronic transitions are revealed originating from $^4F_{9/2} \rightarrow {}^6H_{15/2}$, $^4F_{9/2} \rightarrow {}^6H_{13/2}$, $^4F_{9/2} \rightarrow {}^6H_{11/2}$, and $^4F_{9/2} \rightarrow {}^6H_{9/2}$ transitions (Figure S3). The PL emission is realized by an efficient metal to metal energy transfer (ET) process from the Co(III) cyanide complex to the Dy(III) ion and a moderate ET from $bpyO_2$ ligands to Dy(III) due to the energy back transfer process (BET) between the excited states of similar energy of the ligand and the Dy(III) ion (Figure 7).[53,54] This is the main reason that no sensitization of the Dy(III) emission is observed for temperatures higher than 280 K (Figure S4). Considering the case of **2**, the excited carriers are quenched in Fe(III) resulting in an emission govern by the $bpyO_2$ ligand only with a peak at 440 nm (Figure S4).

For the case of **1**, a high resolution emission spectrum of the $^4F_{9/2} \rightarrow {}^6H_{15/2}$ transition under UV excitation (375 nm) was observed at 10 K which was used for a magneto optical correlation with the energy splitting of the $^6H_{15/2}$ derived from the *ab initio* calculations and the ac magnetic measurements. The deconvolution of the spectrum was succeeded with an 11 components multi Gaussian function. The number of components of this multi Gaussian function was decided after careful assignment of three hot bands in the PL spectrum. The emission PL spectra of the $^4F_{9/2} \rightarrow {}^6H_{15/2}$ transition for **1** at different operating temperatures, deconstructed via 11 components multi Gaussian function from 10−200 K, is also shown in Figure S5. In a typical emission spectrum of the $^4F_{9/2} \rightarrow {}^6H_{15/2}$ transition, eight peaks (red colored transitions and Gaussian peaks in Figure 8) are expected, denoting the transitions from the lowest m_J level of the excited $^4F_{9/2}$ Stark multiplet to the eight (8) m_J levels of the ground multiplet $^6H_{15/2}$. Three extra peaks are also present in the spectrum revealing the presence of three transitions arising from "hot" bands involving the second (blue colored transitions and Gaussian peaks in Figure 8) Stark sublevels of the $^4F_{9/2}$. The assignment of the hot peaks is based on the temperature dependence of the PL emission spectrum where the intensity of the peaks in the area 20 700−20 950 cm^{-1} is increased from 20 to 240 K.

The assignment of the transitions is shown in Table S8 as well as the comparison between the energy spectrum of the Stark sublevels obtained from the PL studies and the *ab initio* calculations. The same comparison is shown graphically in the Figure 8. According to the PL studies and taking into consideration the fact that an Orbach mechanism is expected to describe the relaxation of the magnetization involving the first excited Kramers doublet, the energy separation between these peaks provides a safe ground to estimate the zero field energy barrier.

The presence of temperature dependent hot bands is demonstrated in the emission spectra presented in Figure 9a,b, suggesting the possibility for optical thermometry applications. To estimate the relative thermal sensitivities in **1**, it is possible to employ two different approaches. The first case involves band transitions $^4F_{9/2} \rightarrow {}^6H_{15/2}$ in Figure 10a, where I_1 = 20 735−20 785 cm^{-1} and I_2= 20 882−20 937 cm^{-1}. The thermoelectric parameter (Δ) can be estimated via monitoring the ratio of I_1 and I_2 over the temperature, where Δ can be fit by applying a Mott−Seitz model as shown in eq 1 below

$$\Delta(T) = \Delta_0/[1 + \alpha_1 e^{-\Delta E_1/\kappa_B T} + \alpha_2 e^{-\Delta E_2/\kappa_B T}] \quad (1)$$

where Δ_0 is the thermometric parameter at T = 0 K, α_i (i = 1−2) are the ratios between nonradiative and radiative rates, and ΔE_i (i = 1−2) are the activation energies for nonradiative channels. The parameters are presented in Table 1.

The thermal relative sensitive was obtained via eq 2:[55]

$$S_r = [(d\Delta/dT)/\Delta] \times 100 \quad (2)$$

where the first term is the first order derivative of the function and the second term is the fitted Δ values. This approach results in maximum relative sensitivity of 0.2% K^{-1}at 90 K as shown in Figure 9e. The second case involves band transitions $^4F_{9/2} \rightarrow {}^6H_{13/2}$ in Figure 10b, where I_1 = 17 130−17 230 cm^{-1} and I_2 = 17 624−17 720 cm^{-1}. The latter results in relative maximum thermal sensitivity of 1.84% K^{-1} at 70 K, which is higher than the acceptable sensitivity boundary of 1% K^{-1} for high performance luminescence thermometers,[56,57] in a broad range of temperature between 40 and 140 K.

Figure 10a,b presents the temperature dependent PL spectra of crystalline compounds **2** and **1**, respectively. The overall emission of **2** results in a "bluish" color as presented by the CIE 1931 diagram in Figure 10c, with the emission shifting toward blue with increasing temperature, as presented in Figure 10e. In contrast, the use of the Co(III) cyanide complex in **1** results in the energy transfer to Dy(III) emissive state as can be seen in Figure 10b. The high resolution spectra in Figure 10b reveals the narrow transitions assigned to the f−f states of Dy(III) along with the three characteristics set of emission peaks centered at 480, 580, and 665 nm.[56,58] A more whitish color is presented in the CIE 1931 diagram in Figure 10d, with the effect of the environmental conditions being less pronounced in terms of the (x, y) coordinates as shown in

Figure 10f. The detailed (x, y) coordinates are presented in Table S9 for both samples. The inset graph of Figure 10f presents the correlated color temperature of **1**, revealing a temperature shift from warm white (3200 K) at 10 K toward a more natural white color near 4000 K at room temperature, enabling potential applications for solid state lighting.

CONCLUSIONS

We reported a new multifunctional heterodinuclear compound $[DyCo^{III}(CN)_6(bpyO_2)_2(H_2O)_3]\cdot 4H_2O$, **1**, featuring SMM magnetic properties and temperature dependent photolumi nescent characteristics. In a parallel manner, another heterodinuclear complexes $[DyFe^{III}(CN)_6(bpyO_2)_2(H_2O)_3]\cdot 4H_2O$, **2**, is also presented featuring SMM properties upon application of a dc field. Through SQUID, μ SQUID, and CASSCF calculations, we find the systems to possess similar high temperature relaxation dynamics, while the dynamics at lower temperatures differ strongly. For **1**, the relaxation properties are contingent upon the Dy(III) magnetic characteristics, while for **2**, the dynamics correspond to an antiferromagnetically coupled Dy···Fe pair. The temperature dependent hot bands in the emission spectra of compound **1** have been investigated, and the relative thermal sensitivities have been calculated using two different approaches. A maximum thermal sensitivity of 1.84% K^{-1} at 70 K was calculated, which is higher than the acceptable sensitivity boundary of 1% K^{-1} for high performance luminescence thermometers. Further optical studies focused on the chromaticity diagram of compound **1** revealed a temperature shift from warm white (3200 K) at 10 K toward a more natural white color near 4000 K at room temperature, enabling potential applications of compound **1** for solid state lighting.

ASSOCIATED CONTENT

Supporting Information

The Supporting Information is available free of charge at https://pubs.acs.org/doi/10.1021/acs.inorgchem.1c03432.

Experimental section, IR spectra, crystal structures, theoretical calculations, high resolution optical data (PDF)

Accession Codes

CCDC 2119824 and 2119825 contain the supplementary crystallographic data for this paper. These data can be obtained free of charge via www.ccdc.cam.ac.uk/data request/cif, or by emailing data request@ccdc.cam.ac.uk, or by contacting The Cambridge Crystallographic Data Centre, 12 Union Road, Cambridge CB2 1EZ, UK; fax: +44 1223 336033.

AUTHOR INFORMATION

Corresponding Authors

Vassilis Tangoulis − *Department of Chemistry, University of Patras, 26504 Patras, Greece;* orcid.org/0000 0002 2039 2182; Email: vtango@upatras.gr

Grigorios Itskos − *Experimental Condensed Matter Physics Laboratory, Department of Physics, University of Cyprus, Nicosia 1678, Cyprus;* orcid.org/0000 0003 3971 3801; Email: itskos@ucy.ac.cy

Wolfgang Wernsdorfer − *Institute for Quantum Materials and Technology (IQMT), Karlsruhe Institute of Technology (KIT), D 76344 Eggenstein Leopoldshafen, Germany; Physikalisches Institut, Karlsruhe Institute of Technology, D 76131 Karlsruhe, Germany;* orcid.org/0000 0003 4602 5257; Email: wolfgang.wernsdorfer@kit.edu

Authors

Vassilis Nastopoulos − *Department of Chemistry, University of Patras, 26504 Patras, Greece*

Nikos Panagiotou − *Department of Chemistry, University of Cyprus, Nicosia 1678, Cyprus*

Anastasios Tasiopoulos − *Department of Chemistry, University of Cyprus, Nicosia 1678, Cyprus;* orcid.org/0000 0002 4804 3822

Modestos Athanasiou − *Experimental Condensed Matter Physics Laboratory, Department of Physics, University of Cyprus, Nicosia 1678, Cyprus;* orcid.org/0000 0003 1684 9482

Eufemio Moreno Pineda − *Depto. de Química Física, Escuela de Química, Facultad de Ciencias Naturales, Exactas y Tecnología, Universidad de Panamá, Panamá 18233, Panamá*

Michael Schulze − *Physikalisches Institut, Karlsruhe Institute of Technology, D 76131 Karlsruhe, Germany;* orcid.org/0000 0002 7169 0630

Ondřej Malina − *Regional Centre of Advanced Technologies and Materials, Czech Advanced Technology and Research Institute (CATRIN), Palacký University Olomouc, Olomouc 771 47, Czech Republic*

Complete contact information is available at: https://pubs.acs.org/10.1021/acs.inorgchem.1c03432

Notes

The authors declare no competing financial interest.

ACKNOWLEDGMENTS

O.M. thanks the support of the ERDF/ESF project "Nano4 Future" (No. CZ.02.1.01/0.0/0.0/16 019/0000754) of the Ministry of Education, Youth and Sports of the Czech Republic. EMP thanks the Panamanian National System of Investigators (SNI, SENACYT) for support. W.W. thanks the A. v. Humboldt foundation and the ERC grant MoQuOS No. 741276.

REFERENCES

(1) Quahab, L., Ed. *Multifunctional Molecular Materials*; Pan Stanford Publishing: Singapore, 2013.

(2) Wang, J.; Zakrzewski, J. J.; Heczko, M.; Zychowicz, M.; Nakagawa, K.; Nakabayashi, K.; Sieklucka, B.; Chorazy, S.; Ohkoshi, S. i. Proton Conductive Luminescent Thermometer Based on Near Infrared Emissive {$YbCo_2$} Molecular Nanomagnets. *J. Am. Chem. Soc.* **2020**, *142*, 3970−3979.

(3) Sessoli, R.; Boulon, M. E.; Caneschi, A.; Mannini, M.; Poggini, L.; Wilhelm, F.; Rogalev, A. Strong magneto chiral dichroism in a paramagnetic molecular helix observed by hard X rays. *Nat. Phys.* **2015**, *11*, 69−74.

(4) Ferrando Soria, J.; Khajavi, H.; Serra Crespo, P.; Gascon, J.; Kapteijn, F.; Julve, M.; Lloret, F.; Pasan, J.; Ruiz Perez, C.; Journaux, Y.; Pardo, E. Highly Selective Chemical Sensing in a Luminescent Nanoporous Magnet. *Adv. Mater.* **2012**, *24*, 5625−5629.

(5) Lochenie, C.; Schötz, K.; Panzer, F.; Kurz, H.; Maier, B.; Puchtler, F.; Agarwal, S.; Köhler, A.; Weber, B. Spin Crossover Iron(II) Coordination Polymer with Fluorescent Properties: Correlation between Emission Properties and Spin State. *J. Am. Chem. Soc.* **2018**, *140*, 700−709.

(6) Pedersen, K. S.; Perlepe, P. S.; Aubrey, M. L.; Woodruff, D. N.; Reyes Lillo, S. E.; Reinholdt, A.; Voigt, L.; Li, Z.; Borup, K.; Rouzieres, M.; et al. Formation of the layered conductive magnet

$CrCl_2(pyrazine)_2$ through redox active coordination chemistry. *Nat. Chem.* **2018**, *10*, 1056−1061.
(7) Darawsheh, M.; Barrios, L. A.; Roubeau, O.; Teat, S. J.; Aromi, G. Encapsulation of a Cr^{III} single ion magnet within an Fe^{II} spin crossover supramolecular host. *Angew. Chem., Int. Ed.* **2018**, *57*, 13509−13513.
(8) Long, J. Luminescent Schiff Base Lanthanide Single Molecule Magnets: The Association Between Optical and Magnetic Properties. *Front. Chem.* **2019**, *7*, 00063.
(9) See the various reviews in Martin Ramos, P., Ramos Silva, M.,, Eds. *Lanthanide Based Multifunctional Materials*; Elsevier: Amsterdam, The Netherlands, 2018.
(10) Huskowska, E.; Turowska Tyrk, I.; Legendziewicz, J.; Riehl, J. P. The structure and spectroscopy of lanthanide(III) complexes with 2,2′ bipyridine 1,1′ dioxide in solution and in the solid state: effects of ionic size and solvent on photophysics, ligand structure and coordination. *New J. Chem.* **2002**, *26*, 1461−1467.
(11) Zakrzewski, J. J.; Chorazy, S.; Nakabayashi, K.; Ohkoshi, S. i.; Sieklucka, B. Photoluminescent Lanthanide(III) Single Molecule Magnets in Three Dimensional Polycyanidocuprate(I) Based Frame works. *Chem. Eur. J.* **2019**, *25*, 11820−11825.
(12) Eliseeva, S. V.; Pleshkov, D. N.; Lyssenko, K. A.; Lepnev, L. S.; Bünzli, J. C. G.; Kuzmina, N. P. Deciphering Three Beneficial Effects of 2,2′ Bipyridine N,N′ Dioxide on the Luminescence Sensitization of Lanthanide(III) Hexafluoroacetylacetonate Ternary Complexes. *Inorg. Chem.* **2011**, *50*, 5137−5144.
(13) Beedle, C. C.; Stephenson, C. J.; Heroux, K. J.; Wernsdorfer, W.; Hendrickson, D. N. Photoluminescent Mn_4 Single Molecule Magnet. *Inorg. Chem.* **2008**, *47*, 10798−10800.
(14) Mamontova, E.; Long, J.; Ferreira, R. A. S.; Botas, A. M. P.; Luneau, D.; Guari, Y.; Carlos, L. D.; Larionova, J. Magneto Luminescence Correlation in the Textbook Dysprosium(III) Nitrate Single Ion Magnet. *Magnetochemistry* **2016**, *2*, 41.
(15) Long, J.; Vallat, R.; Ferreira, R. A. S.; Carlos, L. D.; Almeida Paz, F. A.; Guari, Y.; Larionova, J. A bifunctional luminescence single ion magnet: Towards correlation between luminescence studies and magnetic slow relaxation processes. *Chem. Commun.* **2012**, *48*, 9974−9976.
(16) Yamashita, K.; Miyazaki, R.; Kataoka, Y.; Nakanishi, T.; Hasegawa, Y.; Nakano, M.; Yamamura, T.; Kajiwara, T. A luminescent single molecule magnet: Observation of magnetic anisotropy using emission as a probe. *Dalton Trans.* **2013**, *42*, 1987−1990.
(17) Pointillart, F.; Le Guennic, B.; Golhen, S.; Cador, O.; Maury, O.; Ouahab, L. A redox active luminescent ytterbium based single molecule magnet. *Chem. Commun.* **2013**, *49*, 615−617.
(18) Gavey, E. L.; AlHareri, M.; Regier, J.; Carlos, L. D.; Ferreira, R. A. S.; Razavi, F. S.; Rawson, J. M.; Pilkington, M. Placing a crown on Dy(III) A dual property Ln^{III} crown ether complex displaying optical properties and SMM behaviour. *J. Mater. Chem. C* **2015**, *3*, 7738−7747.
(19) For an excellent recent review, see Marin, R.; Brunet, G.; Murugesu, M. Shining new light on multifunctional lanthanide single molecule mangets. *Angew. Chem., Int. Ed.* **2021**, *60*, 1728−1746.
(20) Quintanilla, M.; Liz Marzán, L. M. Guiding Rules for Selecting a Nanothermometer. *Nano Today* **2018**, *19*, 126−145.
(21) Errulat, D.; Marin, R.; Gálico, D. A.; Harriman, K. L. M.; Pialat, A.; Gabidullin, B.; Iikawa, F.; Couto, O. D. D., Jr.; Moilanen, J. O.; Hemmer, E.; Sigoli, F. A.; Murugesu, M. A Luminescent Thermometer Exhibiting Slow Relaxation of the Magnetization: Toward Self Monitored Building Blocks for Next Generation Optomagnetic Devices. *ACS. Cent. Sci.* **2019**, *5*, 1187−1198.
(22) Liu, K.; Shi, W.; Cheng, P. Toward heterometallic Single molecule magnets: Synthetic strategy, structures and properties of 3d 4f discrete complexes. *Coord. Chem. Rev.* **2015**, *289*−*290*, 74−192.
(23) Dey, A.; Acharya, J.; Chandrasekhar, V. Heterometallic 3d 4f Complexes as Single Molecule Magnets. *Chem. Asian J.* **2019**, *14*, 4433−4453.
(24) Rosado Piquer, L.; Sañudo, E. C. Heterometallic 3d/4f single molecule magnets. *Dalton Trans.* **2015**, *44*, 8771−8780.
(25) Sharples, J. W.; Collison, D. The coordination chemistry and magnetism of some 3d/4f amino polyalcohol compounds. *Coord. Chem. Rev.* **2014**, *260*, 1−20.
(26) Feltham, H. L. C.; Brooker, S. Review of purely 4f and mixed metal nd 4f single molecule magnets containing only one lanthanide ion. *Coord. Chem. Rev.* **2014**, *276*, 1−33.
(27) Brunet, G.; Marin, R.; Monk, M. J.; Resch Genger, U.; Gálico, D. A.; Sigoli, F. A.; Suturina, E. E.; Hemmer, E.; Murugesu, M. Exploring the dual functionality of an ytterbium complex for luminescence thermometry and slow magnetic relaxation. *Chem. Sci.* **2019**, *10*, 6799−6808.
(28) Beltran, L. M.; Long, J. R. Directed assembly of metal cyanide cluster magnets. *Acc. Chem. Res.* **2005**, *38*, 325−334.
(29) Sokol, J. J.; Hee, A. G.; Long, J. R. A cyano bridged single molecule magnet: Slow magnetic relaxation in a trigonal prismatic $MnMo_6(CN)_{18}$ cluster. *J. Am. Chem. Soc.* **2002**, *124*, 7656−7657.
(30) Wang, X. Y.; Avendaño, C.; Dunbar, K. R. Molecular magnetic materials based on 4d and 5d transition metals. *Chem. Soc. Rev.* **2011**, *40*, 3213−3238.
(31) Pinkowicz, D.; Podgajny, R.; Nowicka, B.; Chorazy, S.; Reczynski, M.; Sieklucka, B. Magnetic clusters based on octacyani dometallates. *Inorg. Chem. Front.* **2015**, *2*, 10−27.
(32) Wang, J. H.; Li, Z. Y.; Yamashita, M.; Bu, X. H. Recent progress on cyano bridged transition metal based single molecule magnets and single chain magnets. *Coord. Chem. Rev.* **2021**, *428*, 213617.
(33) Chorazy, S.; Rams, M.; Wang, J.; Sieklucka, B.; Ohkoshi, S. i. Octahedral Yb(III) complexes embedded in $[Co(CN)_6]$ bridged coordination chains: combining sensitized near infrared fluorescence with slow magnetic relaxation. *Dalton Trans.* **2017**, *46*, 13668−13672.
(34) Xin, Y.; Wang, J.; Zychowicz, M.; Zakrzewski, J. J.; Nakabayashi, K.; Sieklucka, B.; Chorazy, S.; Ohkoshi, S. i. i. Dehydration Hydration Switching of Single Molecule Magnet Behav ior and Visible Photoluminescence in a Cyanido Bridged $Dy^{III}Co^{III}$ Framework. *J. Am. Chem. Soc.* **2019**, *141*, 18211−18220.
(35) Chorazy, S.; Rams, M.; Nakabayashi, K.; Sieklucka, B.; Ohkoshi, S. i. White Light Emissive DyIII Single Molecule Magnets Sensitized by Diamagnetic $[Co^{III}(CN)_6]^{3-}$ Linkers. *Chem. Eur. J.* **2016**, *22*, 7371−7375.
(36) Gao, S.; Ma, B.; Wang, Z.; Yi, T.; Liao, C.; Yan, C.; Xu, G. Structure and Magnetism of Cyano Bridged Hetero Binuclear Complexes $RE(dpdo)_2(H_2O)_3Fe(CN)_6{\cdot}4H_2O$ (RE = Gd, Y). *Mol. Cryst. Liq. Cryst.* **1999**, *335*, 201−210.
(37) Yan, B.; Song, Y. A Novel Water Soluble 4f 3d Heterometallic Cyano bridged Complex, $Sm(bpyO_2)_2(H_2O)_3Fe(CN)_6{\cdot}4H_2O$. *J. Coord. Chem.* **2004**, *57*, 49−54.
(38) Pilichos, E.; Spanakis, E.; Maniaki, E. K.; Raptopoulou, C. P.; Psycharis, V.; Turnbull, M. M.; Perlepes, S. P. Diversity of Coordination Modes in a Flexible Ditopic Ligand Containing 2 pyridyl, Carbonyl and Hydrazone Functionalities: Mononuclear and Dinuclear Cobalt(III) Complexes, and Tetranuclear Copper(II) and Nickel(II) Clusters. *Magnetochemistry* **2019**, *5*, 39.
(39) Nakamoto, K. *Infrared and Raman Spectra of Inorganic and Coordination Compounds*, 4th ed.; Wiley: New York, 1986; pp. 107, 272−280.
(40) Nakagawa, I.; Shimanouchi, T. Infrared spectroscopic study on the co ordination bond II. Infrared spectra of octahedral metal cyanide complexes. *Spectrochim. Acta* **1962**, *18*, 101−113.
(41) Kanno, H.; Omotera, Y.; Iijima, K. 2,2′ Bipyridine 1,1′ Dioxide. *Acta Crystallogr., Sect. C: Cryst. Struct. Commun.* **1998**, *54*, 149−151.
(42) Bodige, S. G.; Zottola, M. A.; McKay, S. E.; Blackstock, S. G. Heterocyclic N oxide CH···O Hydrogen Bonding (Part 3). Crystal Packing of 2,2′ Bipyridine 1,1′ dioxide and Pyridine N oxide. *Cryst. Eng.* **1998**, *1*, 243−253.
(43) Llunell, M.; Casanova, D.; Girera, J.; Alemany, P.; Alvarez, S. *SHAPE: Program for the Stereochemical Analysis of Molecular Fragments by Means of Continuous Shape Measures and Associated Tools*, v 2.1; University of Barcelona, Barcelona, 2013.

(44) Kepert, D. L. *Inorganic Stereochemistry*; Springer Verlag: New York, 1982.
(45) For example, see Al Karaghouli, A. R.; Day, R. O.; Wood, J. S. Crystal Structure of Tetrakis(2,2′ bipyridine dioxide)lanthanum Perchlorate: An Example of Cubic Eight Coordination. *Inorg. Chem.* **1978**, *17*, 3702−3706.
(46) Aquilante, F.; Autschbach, J.; Carlson, R. K.; Chibotaru, L. F.; Delcey, M. G.; De Vico, L.; Fdez. Galván, I.; Ferré, N.; Frutos, L. M.; Gagliardi, L.; et al. Molcas 8: New capabilities for multiconfigurational quantum chemical calculations across the periodic table. *J. Comput. Chem.* **2016**, *37*, 506−541.
(47) Roos, B. O.; Lindh, R.; Malmqvist, P. Å.; Veryazov, V.; Widmark, P. O. Main Group Atoms and Dimers Studied with a New Relativistic ANO Basis Set. *J. Phys. Chem. A* **2004**, *108*, 2851−2858.
(48) Roos, B. O.; Lindh, R.; Malmqvist, P. Å.; Veryazov, V.; Widmark, P. O. New Relativistic ANO Basis Sets for Transition Metal Atoms. *J. Phys. Chem. A* **2005**, *109*, 6575−6579.
(49) Lunghi, A.; Totti, F.; Sessoli, R.; Sanvito, S. The role of anharmonic phonons in under barrier spin relaxation of single molecule magnets. *Nat. Commun.* **2017**, *8*, 14620.
(50) Wei, R. M.; Liu, T.; Li, J.; Zhang, X.; Chen, Y.; Zhang, Y. Q. Tuning the Magnetization Dynamic Properties of NdFe and NdCo Single Molecular Magnets by Introducing 3 d 4 f Magnetic Interactions. *Chem. Asian J.* **2019**, *14* (11), 2029−2035.
(51) Stoian, S. A.; Paraschiv, C.; Kiritsakas, N.; Lloret, F.; Munck, E.; Bominaar, E. L.; Andruh, M. Mossbauer, electron paramagnetic resonance, and magnetic susceptibility studies on members of a new family of cyano bridged 3d 4f complexes. Demonstration of anisotropic exchange in a Fe Gd complex. *Inorg. Chem.* **2010**, *49* (7), 3387−401.
(52) Abouelwafa, A. S.; Mereacre, V.; Balaban, T. S.; Anson, C. E.; Powell, A. K. Photo and thermally enhanced charge separation in supramolecular viologen hexacyanoferrate complexes. *CrystEngComm* **2010**, *12* (1), 94−99.
(53) Zakrzewski, J. J.; Chorazy, S.; Nakabayashi, K.; Ohkoshi, S.; Sieklucka, B. Photoluminescent Lanthanide(III) Single Molecule Magnets in Three Dimensional Polycyanidocuprate(I) Based Frame works. *Chem. Eur. J.* **2019**, *25*, 11820.
(54) Eliseeva, V. S.; Pleshkov, N. D.; Lyssenko, A. K.; Lepnev, S. L.; Bünzli, G. J. C.; Kuzmina, P. N. Deciphering Three Beneficial Effects of 2,2′ Bipyridine *N,N′* Dioxide on the Luminescence Sensitization of Lanthanide(III) Hexafluoroacetylacatonate Ternary Complexes. *Inorg. Chem.* **2011**, *50*, 5137−5144.
(55) Kitos, A. A.; Gálico, D. A.; Castañeda, R.; Ovens, J. S.; Murugesu, M.; Brusso, J. L. Stark Sublevel Based Thermometry with Tb(III) and Dy(III) Complexes Cosensitized via the 2 Amidinopyr idine Ligand. *Inorg. Chem.* **2020**, *59*, 11061−11070.
(56) Zhong, L.; Chen, W. B.; Li, X. H.; Ouyang, Z. J.; Yang, M.; Zhang, Y. Q.; Gao, S.; Dong, W. Four Dinuclear and One Dimensional Chain Dysprosium and Terbium Complexes Based on 2 Hydroxy 3 Methoxybenzoic Acid: Structures, Fluorescence, Single Molecule Magnet, and Ab Initio Investigation. *Inorg. Chem.* **2020**, *59*, 4414−4423.
(57) Cucinotta, G.; Perfetti, M.; Luzon, J.; Etienne, M.; Car, P. E.; Caneschi, A.; Calvez, G.; Bernot, K.; Sessoli, R. Magnetic Anisotropy in a Dysprosium/DOTA Single Molecule Magnet: Beyond Simple Magneto Structural Correlations. *Angew. Chemie Int. Ed.* **2012**, *51* (7), 1606−1610.
(58) Chorazy, S.; Wang, J.; Ohkoshi, S. I. Yellow to Greenish Blue Colour Tunable Photoluminescence and 4f Centered Slow Magnetic Relaxation in a Cyanido Bridged DyIII(4 Hydroxypyridine) CoIII Layered Material. *Chem. Commun.* **2016**, *52* (71), 10795−10798.